Macromolecular proton fraction mapping of the human liver *in vivo*: technical feasibility and preliminary observations in hepatic fibrosis

V. L. Yarnykh[1], and G. N. Ioannou[2]
[1]Department of Radiology, University of Washington, Seattle, WA, United States, [2]Department of Medicine, University of Washington, Seattle, WA, United States

Introduction: Cross-relaxation imaging (CRI) is a new quantitative MRI method, which allows the measurement and *in vivo* mapping of key parameters determining magnetization transfer (MT) between water and macromolecules in tissues (1,2). One of these parameters, macromolecular proton fraction (MPF) is of special interest, since it provides direct measurement of the portion of macromolecular protons causing the MT effect and is indicative of the total content of macromolecules in tissues. Recent studies resulted in the development of several time-efficient technical variants of CRI and demonstrated applications of this technology in neuroimaging (2-4). However, the CRI method has not been adapted for abdominal imaging applications to date. A promising clinical application of MPF mapping is the detection and staging of hepatic fibrosis, which is characterized by the formation of collagen-rich extracellular matrix and results in a dramatic increase of collagen content in the liver (5). Collagen is a highly cross-linked protein, which is known to demonstrate a strong MT effect due to a high MPF (6). The goals of this study were twofold. First, we aimed to develop an ultra-fast technique for liver CRI that would allow breath-hold data acquisition to mitigate motion artifacts. Second, we sought to test the hypothesis that hepatic fibrosis results in an increased MPF in the liver.

Methods: ***Subjects:*** Data were obtained from six patients with chronic hepatitis C virus (HCV) infection who underwent liver biopsy within the preceding 6 months. Hepatic fibrosis was staged according to the METAVIR score. Three subjects had no fibrosis (F0 stage) and served as controls. Other three subjects had different fibrosis stages (F1, F3, and F4).

MRI protocol: A protocol allowing liver CRI data acquisition during four breath-hold intervals was created for a 3T whole-body MRI scanner (Philips Achieva, Best, Netherlands). The overview of image acquisition and processing steps is presented in Fig.1. All data were acquired using 3D sequences with 12 5 mm slices (interpolated from the actual 10 mm thickness) and FOV 400x300 mm^2. Four MT-weighted data points were acquired in a single breath-hold interval using a spoiled MT-prepared multi-shot EPI gradient-echo sequence with fractional k-space acquisition, TR/TE=69.8/2.3 ms, α=15°, and EPI factor 9. A single-lobe-sinc saturation pulse with Gaussian apodization was applied with the duration 33 ms and saturation flip angle 1000° at four offset frequencies Δ=2, 6, 10, and 96 kHz (reference image used for data normalization). The total scan time was 25 s (6.2 s per point). For complementary T_1 mapping, the variable flip angle (VFA) method was used. VFA data were acquired in a single breath-hold interval using a spoiled gradient-echo sequence (TR/TE=20/2.3 ms) with three flip angles (α=3, 10, and 20°) and the total scan time of 23.4 s (7.8 s per point). The VFA method was implemented with recent spoiling modifications (7) including an optimal combination of the RF phase increment (169°) and spoiling gradient area (A_G=523 mT·ms/m). VFA and MT data were obtained with resolution 2x3x10 mm^3 and interpolated to 1x1x5 mm^3. Additionally, fast sequences for correction of main magnetic field (B_0) and RF field (B_1) non-uniformities were implemented, each with a single-breath-hold acquisition. For B_0 mapping, the dual-echo method (8) was used with TR/TE$_1$/TE$_2$=20/2.3/3.3 ms, α=8°, resolution 2.5x4x10 mm^3, and the scan time 18 s. B_1 maps were obtained using the actual flip angle imaging (AFI) method (9) with improved RF and gradient spoiling (7). The AFI sequence was used with the following parameters: TR$_1$/TR$_2$/TE=17/85/2.3 ms, α=55°, RF phase increment 39°, spoiling gradient areas A_{G1}/A_{G2}=422/2110 mT·ms/m, resolution 2.5x6x10 mm^3, and the scan time 31 s.

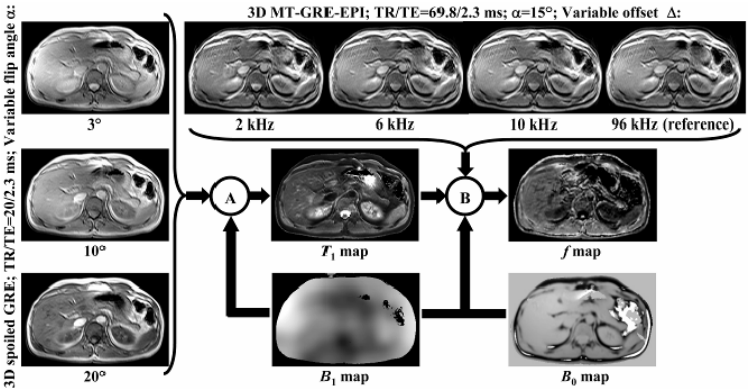

Fig 1. Overview of image acquisition and processing steps in fast MPF mapping of the liver. The entire acquisition protocol is accomplished during four breath-hold intervals. The image processing step (A) corresponds to reconstruction of T_1 maps by fitting the Ernst formula to VFA data with B_1 correction (9). The image processing step (B) corresponds to the single-parameter fit of MPF (f map) based on the matrix pulsed MT model with B_1 and B_0 correction (4).

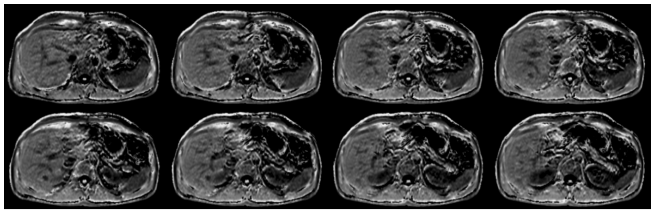

Fig 2. Example MPF maps of the liver obtained from a subject with no fibrosis (stage F0): 8 consecutive 5 mm slices (out of 12) corresponding to the central part of the 3D slab.

Image processing: MPF maps were reconstructed using the single-parameter fit (parameter f) of the matrix model of pulsed MT (1,2) from three data points normalized to the reference image. The single-parameter f fitting procedure was similar to that recently described for the brain (4), while liver-specific constraints for other two-pool model parameters (T_2^B=7.7 μs and R=50 s^{-1}) were based on the literature data for animal liver *ex vivo* (10). The constraint for the product $T_2^F R_1^F$=0.024 was assigned similar to the brain data at 3T (3,4). To avoid errors caused by the slab excitation profile, eight slices corresponding to the central portion of the 3D slab were used in subsequent processing. After reconstruction of MPF maps, the liver was manually segmented, and normalized MPF histograms of the liver parenchyma were computed with the bin size of 0.25%.

Table 1. Liver MPF histogram parameters

Group	Mean / %	$V_{6.5\%}$ / %
Control	6.09±0.09	33.5±2.3
Early fibrosis	6.25	39.7
Advanced fibrosis	6.88±0.06	61.4±2.9

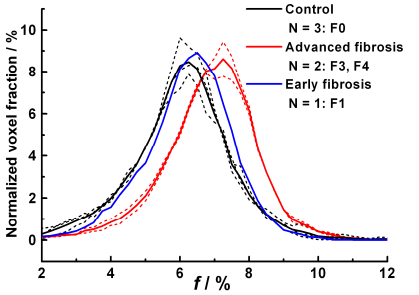

Fig. 3. MPF histograms of the liver. Bold solid plots represent group mean histograms, and thin dashed plots correspond to individual histograms of subjects.

Results: A representative set of MPF maps is shown in Fig. 2. Histograms for all subjects are presented in Fig. 3, and summary data are given in Table 1. The data in Fig. 3 indicate that the MPF histograms demonstrate shift to higher values with an increase of the fibrosis stage. Position of MPF histograms of control subjects appears highly consistent, demonstrating rather small deviations around the mean value (Fig. 3 and Table 1). For advanced fibrosis subjects (F3 and F4), the histograms appeared very similar, both dramatically shifted from controls. While a consistent interpretation of the absence of clear distinctions between F3 and F4 subjects is impossible due to limited data, these histograms can be grouped together for the purpose of preliminary MPF estimation in advanced fibrosis. For early fibrosis (F1), a smaller but well visible shift of a histogram to higher MPF values is seen (Fig. 3). Based on the appearance of MPF histograms, two approaches can be suggested for analysis of clinical data: a) a measure of the central tendency (e.g. mean value) and b) a voxel fraction above an appropriate threshold value. As the illustration of the last approach, we have chosen an empiric threshold value of 6.5% ($V_{6.5\%}$), which provides excellent discrimination between groups (Table 1). Both approaches demonstrated significant differences between controls and advanced fibrosis subjects: P=0.002 for the mean values and P=0.001 for $V_{6.5\%}$ by independent t-test.

Conclusions: This study provides the first demonstration of the feasibility of abdominal CRI. Our preliminary clinical data are in good agreement with the hypothesis that MPF is increased in hepatic fibrosis compared to the normal liver parenchyma, and this increase is associated with the fibrosis stage. Further studies with a larger number of subjects are warranted to evaluate MPF as a prospective quantitative imaging biomarker of hepatic fibrosis.

References: (**1**) Yarnykh VL. *MRM* 2002;47:929. (**2**) Yarnykh VL, Yuan C. *Neuroimage* 2004;23:409. (**3**) Underhill HR, et al. *Neuroimage* 2009;47:1568. (**4**) Underhill HR, et al. *Neuroimage* 2010; In press. (**5**) Popper H, Uenfriend S. *Am J Med* 1970;49:707. (**6**) Edzes HT, Samulski ET. *JMR* 1978;31:207. (**7**) Yarnykh VL. *MRM* 2010;63:1610. (**8**) Skinner TE, Glover GH. *MRM* 1997;37:628. (**9**) Yarnykh VL. *MRM* 2007;57:192. (**10**) Stanisz GJ, et al. *MRM* 2005;54:507.